Journal of Inflammation Research

Dovepress
Taylor & Francis Group

Open Access Full Text Article

ORIGINAL RESEARCH

Screening and Targeting the HMGB1/RAGE Axis via Proteomics to Alleviate Inflammatory Responses in a *Pseudomonas aeruginosa*-Induced Rat Model of VAP

Xuanli Huang[1,*], Mingpeng Feng[2,*], Siqi Li[1], Chengjun Huang[1], Yu Xu[1], Haifei Cheng[1], Le Mi[1], Hongman Wang[1]

[1]The Fifth Affiliated (Zhuhai) Hospital of Zunyi Medical University, Zunyi Medical University, Zhuhai, Guangdong, People's Republic of China; [2]Medicine & Technology College Oof Zunyi Medical University, Zunyi Medical University, Zunyi, Guizhou, People's Republic of China

*These authors contributed equally to this work

Correspondence: Hongman Wang, The Fifth Affiliated (Zhuhai) Hospital of Zunyi Medical University, Zunyi Medical University, Doumen District, Zhuhai, Guangdong, 519100, People's Republic of China, Tel +86-0756-6275976, Email 2496453591@qq.com

Purpose: Ventilator-associated pneumonia (VAP) is a common and serious complication in mechanically ventilated patients, with *Pseudomonas aeruginosa* (PA) being one of the most frequently encountered pathogens. Dysregulated protein expression is closely associated with the progression of VAP; therefore, identifying and modulating potential protein targets are crucial for developing novel therapeutic strategies.

Methods: Quantitative proteomics was employed to analyze protein expression changes in a PA-induced rat model of VAP. Bioinformatics analysis was performed to identify key signaling pathways and potential small-molecule inhibitors. Immuno-infiltration analysis and immunofluorescence co-localization assays were conducted on rat lung tissues. The expression levels of HMGB1, RAGE, TNF-α, IL-1β, and IL-6 in bronchoalveolar lavage fluid (BALF) and blood were measured using ELISA.

Results: PA infection induced the upregulation of the HMGB1/RAGE axis. Bioinformatics analysis indicated that the HMGB1/RAGE axis is involved in key pathways such as neutrophil extracellular trap (NET) formation and identified potential small-molecule inhibitors, including potassium nitrate and 2-mercaptoethanol. Immuno-infiltration analysis revealed a negative correlation between the HMGB1/RAGE axis and monocytes. FPS-ZM1-treated rats showed reduced co-expression of HMGB1 and RAGE in lung tissue, decreased levels of HMGB1, RAGE, TNF-α, IL-1β, and IL-6 in BALF and blood, and attenuated systemic inflammatory responses.

Conclusion: These results suggest that the HMGB1/RAGE axis is associated with the inflammatory response in a PA-induced rat model of VAP, and that blocking this interaction with FPS-ZM1 alleviates both lung injury and systemic inflammation.

Keywords: ventilator-associated pneumonia, high-mobility group box 1, receptor for advanced glycation end products, *Pseudomonas aeruginosa*, proteomics

Introduction

Ventilator-associated pneumonia (VAP) is one of the most common nosocomial infections in the intensive care unit (ICU), frequently occurring in mechanically ventilated patients. Despite advances in pharmacological treatment and preventive strategies, VAP still carries a mortality rate of 30–50%.[1,2] The VAP is complex. Previous studies have revealed that mechanical ventilation can induce lung injury by activating signaling pathways in endothelial or inflammatory cells, which leads to the substantial release of inflammatory mediators. These mediators not only accumulate in the lungs to cause local tissue damage but can also elicit a systemic inflammatory response.[3–5] Currently, the management of the cytokine storm-like effect in VAP patients, triggered by damage-associated molecular patterns (DAMPs) or

https://doi.org/10.2147/JIR.S580972
Received: 18 November 2025
Accepted: 23 April 2026
Published: 9 May 2026

pathogen-associated molecular patterns (PAMPs) following intubation, poses a significant therapeutic challenge, as empirical antibiotic use and preventive strategies show limited efficacy; therefore, identifying and blocking key pro-inflammatory targets are crucial.

HMGB1 is a multifunctional non-histone nuclear protein that exerts different functions depending on its subcellular localization.[6] Upon stimulation by external "danger signals", HMGB1 can translocate to the extracellular space, where it mediates the pathogenesis of a spectrum of diseases including autoimmune, cardiovascular, and neurodegenerative diseases, metabolic disorders, cancer, and ischemia-reperfusion injury.[7–12]

Accumulating evidence indicates that HMGB1 also plays a critical role in regulating inflammatory responses.[13,14] RAGE is an inflammatory type I transmembrane receptor that is widely distributed in endothelial cells, mononuclear macrophages, lymphocytes, and other cells.[15] RAGE is most abundantly expressed in lung tissue, where it is localized to the basolateral membranes of type I alveolar cells, mediating the connection between type I alveolar epithelial cells (AT-1) and the pulmonary basement membrane. As a multiligand receptor, RAGE recognizes both PAMPs, such as lipopolysaccharide (LPS), microbial DNA, and respiratory viruses, and DAMPs.[16,17] Among these, HMGB1 is the highest-affinity ligand for RAGE, mediating pro-inflammatory intracellular signaling, chemotaxis, and NF-κB activation, thereby promoting neutrophil recruitment and cytokine release. Therefore, the HMGB1/RAGE axis likely plays a significant role in the inflammatory response within the PA-induced rat model of VAP.

Utilizing quantitative liquid chromatography-tandem mass spectrometry (LC-MS/MS), this study performed a comprehensive proteomic analysis on a rat model of VAP induced by PA. The analysis revealed elevated levels of HMGB1 and RAGE alongside aggravated pulmonary and systemic inflammation. However, blockade of the HMGB1/RAGE axis alleviated both local and systemic inflammatory responses.

Materials and Methods

Experimental Animals

Male healthy SPF-grade Sprague-Dawley (SD) adult rats were purchased from Zhuhai Baishitong Biological Co. Ltd. (License No: SCXK (Yue) 2020–0051), The rats were housed at a constant temperature (23 ± 1°C) under a 12/12-h light-dark cycle, with free access to food and water. All experimental operations were conducted following the "Guide for the Care and Use of Laboratory Animals" and approved by the Experimental Animal Ethics Committee of the Zunyi Medical University (Approval No: [2023] 2023ZH0042). All experimental procedures and operations were strictly carried out in accordance with the ARRIVE guidelines.

Strain Preparation

The *Pseudomonas aeruginosa* strain was obtained from a standard strain library, resuscitated and cultured in LB broth to form a standard bacterial suspension. The bacterial concentration was measured using the McFarland turbidity standard, adjusted to approximately $5\times10^{\wedge7}$cfu/mL, ensuring consistent and accurate bacterial concentration for subsequent experiments.

Model Preparation

After a 2-week acclimatization period, the rats were prepared for the experiment. The ventilator settings were adjusted to the following parameters: a tidal volume (VT) of 8 mL/kg, an inspiratory to expiratory ratio of 1:2, a respiratory rate of 80 breaths/min, a positive end-expiratory pressure of 0 cmH2O, an inspired oxygen concentration of 21%, and an inspiratory pause time of 0.5 seconds.[18] The rats were anesthetized by intraperitoneal injection of ethyl carbamate (0.5 mL/100 g) and mechanically ventilated for 2 hours, followed by immediate tracheal instillation of 100 μL of PA ($5\times10\wedge7$ cfu/mL). Thirty minutes later, 20 mL of PBS was injected intraperitoneally. During mechanical ventilation, the rats' lip color and body temperature were carefully monitored to prevent asphyxiation and mortality. At 24 hours post-infection, rats weighing between 250 and 300 g were euthanized by cervical dislocation under deep anesthesia, and samples were collected for analysis.[19,20] The control group rats did not receive tracheal instillation of PA, but were administered the same dose of PBS.

Grouping

Differential Proteomics

Seven rats were randomly divided into two groups: control group (n=3) and VAP model group (PA, n=4). After model establishment, serum was collected from the rats for proteomic analysis.

Study on HMGB1/RAGE as a Therapeutic Target

Eighteen rats were randomly divided into three groups, with each group containing six rats: group, control (control, n=6), group, PA (PA, n=6), group, FPS-ZM1 treatment (FPS-ZM1+PA, n=6). Samples of serum, BALF, and lung tissue were collected 24 hours after modeling. After 2 hours of mechanical ventilation with FPS-ZM1+PA, 100μL of PA (5×10^7 cfu/mL) was administered intratracheally,[19,20] followed by intraperitoneal injection of 20mL FPS-ZM1 after 30 minutes. The dose of FPS-ZM1 was chosen according to previous studies and preliminary experimental results.[21]

Proteomics

Protein Processing

Serum from VAP rats was thawed after being stored at −80°C, and the supernatant was collected after centrifugation. The samples were then pooled, high-abundance proteins were removed, and the samples were diluted for further use. Protein concentration was determined using the BCA method, and a standard curve was prepared to calculate the sample concentrations. Twenty micrograms of protein were analyzed by SDS-PAGE, and the samples were assessed for quality after staining with Coomassie Brilliant Blue. One hundred micrograms of protein were subjected to reduction and alkylation, followed by overnight digestion with trypsin at 37°C, after ultrafiltration, the samples were desalted and lyophilized. The lyophilized peptides were dissolved in mobile phase A and subjected to gradient separation by HPLC, with the fractions collected and re-dissolved for further analysis.

Liquid Chromatography-Mass Spectrometry (LC-MS)

Chromatographic separation was performed using a nanoflow HPLC system (Easy-nLC 1000, Thermo Fisher Scientific). The eluted peptides were analyzed by a Q-Exactive HF-X mass spectrometer (Thermo Fisher Scientific). Mobile phase A consisted of water containing 0.1% formic acid, and mobile phase B was 100% acetonitrile containing 0.1% formic acid. For data-dependent acquisition (DDA) mode, a 120-min linear gradient was applied at a flow rate of 300 nL/min. The gradient profile was as follows: 0–1min, 2–5% B; 1–96 min, 5–25% B,; 96–111 min, 25–35% B,; 111–114 min, 35–100% B; 114–120 min 100% B. Full scan was set at a resolution of 120,000 at 200 m/z (350–1650 m/z) with AGC target of 3e6, maximum injection time of 20 ms. MS2 scan was set at a resolution of 15,000 at 200 m/z, with an AGC target of 1e5, a maximum injection time of 100 ms, an isolation window of 1.4 m/z, and a dynamic exclusion time of 30s. For data-independent acquisition (DIA) mode, separation was performed using a 70-min gradient, 0–1 min, 2–5% B; 1–53 min, 5–25% B; 53–60 min, 25–35% B, 60–62 min, 35–100% B; 62–70 min, 100% B. For data-independent acquisition (DIA), a scheme comprising 32 variable isolation windows was employed, covering a mass range from 350 to 1600 m/z. Specifically, the sequential window setup was configured as: 33 m/z*2, 24 m/z*2, 15 m/z*4, 13 m/z*9, 16 m/z*3, 18 m/z*3, 24 m/z*2, 30 m/z*2, 40 m/z*1, 50 m/z*1, 60 m/z*1, 100 m/z*1, 499 m/z*1. The mass spectrometer settings were aligned with the DDA method for full-scan parameters. However, for MS2 scans, the resolution was increased to 30,000 (at 200 m/z) with an AGC target of 5e5. Higher-energy collisional dissociation fragmentation was performed using a normalized collision energy of 27%. This DIA method was applied to analyze rat serum.

Searching the Database

Using Spectronaut software (version 14.4.200727.47784), a spectral library was constructed by searching the DDA data against the UniProt Rattus norvegicus database (release 2024_01) with the thresholds of false discovery rate (FDR) ≤ 1% and unique peptides ≥ 2. The DIA data were subsequently subjected to qualitative and quantitative analysis based on this spectral library.

Differential Protein Screening

Statistical analysis was performed using R software, where significantly differentially expressed proteins (DEPs) were identified by Welch's *t*-test with thresholds of p-value < 0.05 and fold change (FC > 1.5, followed by Kyoto Encyclopedia of Genes and Genomes (KEGG) pathway analysis conducted via the DAVID online tool (https://david.ncifcrf.gov/).

Analysis of Immune Cell Infiltration

To characterize the immune microenvironment features in the rat model of VAP induced by PA, we employed the single-sample gene set enrichment analysis (ssGSEA) algorithm. The immune cell signature gene sets used were primarily sourced from the "C7: immunologic signature gene sets" subset of the MSigDB (Molecular Signatures Database, v7.5.1).[22,23] The analysis was conducted in the R environment using the GSVA package (version 1.48.3). When calling the gsva() function, the method parameter was set to method="ssgsea", and default settings (including$\tau = 0.25$) were applied to calculate enrichment scores for each immune cell type.[24] To further identify immune cell types associated with phenotypes, we performed screening based on the computed immune cell enrichment scores using Pearson correlation analysis and independent samples t-tests, with a significance threshold of $P<0.05$.

Drug-Target Prediction of HMGB1-RAGE

Drug-target interaction prediction for the HMGB1-RAGE axis was performed using the Enrichr online platform (https://maayanlab.cloud/Enrichr/). Potential small molecule inhibitors were screened based on binding affinity scores and experimental evidence from the DrugBank and ChEMBL databases, with significance threshold set at adjusted p-value < 0.05.

Research on Target Blocking

Lung Tissue W/D Measurement

The wet weight was measured immediately after collecting the right middle lung lobe. The tissue was then dried in a 70°C oven for 24 hours to obtain the dry weight, and the wet-to-dry (W/D) weight ratio was calculated.

Histopathological Analysis

Lung tissue processing was performed following a standard protocol, which included fixation, dehydration, embedding, sectioning, staining, and coverslipping, with images captured at appropriate microscope magnifications for subsequent analysis; Scoring of the lung tissue was conducted in a double-blind manner: 0 for no lesions, 1 for lesions < 25%, 2 for lesions ranging from 25% to 50%, 3 for lesions ranging from 50% to 75%, and 4 for lesions > 75%. The cumulative scores were subjected to statistical analysis.[18]

Detection of BALF and Blood Inflammatory Factors

According to the standard protocol (including sample addition, plate washing, and color development), inflammatory factors TNF-α, IL-1β, and IL-6 were measured in rat BALF and blood, with standard curves plotted using standard concentration on the x-axis and OD values on the y-axis, and sample OD values were interpolated to determine protein expression levels.

HMGB1/RAGE Immunofluorescence Co-Localization Analysis

The frozen sections were baked in a 37°C incubator and then gently washed in PBS buffer. This was followed by antigen retrieval, serum blocking by creating hydrophobic barriers, antibody incubation, and nuclear staining with DAPI. Images were finally processed using ImageJ software (version 1.8.0.345).

Statistical Analysis

Data were analyzed using SPSS 29.0 (SPSS Inc., Chicago, IL, USA), GraphPad Prism 10.0 (GraphPad Software, San Diego, CA, USA) and R language (version 4.0). Data that were normally or approximately normally distributed are presented as the mean ± standard deviation ($\bar{x} \pm SD$). Comparisons of means among multiple groups were performed using one-way analysis of variance (one-way ANOVA). If a statistically significant overall difference was detected, post

hoc multiple comparisons were conducted using the Bonferroni method. For data with heterogeneous variances, group comparisons were made using the nonparametric Kruskal–Wallis rank-sum test. Where a significant overall difference was observed, the Benjamini-Krieger-Yekutieli procedure was applied for further multiple comparisons. A P-value of less than 0.05 was considered statistically significant.

Results

Identification of Potential Target Proteins via Proteomic Analysis

To identify key proteins and pathways involved in PA-induced VAP, we performed quantitative proteomic analysis on serum samples from control and VAP model rats. LC-MS/MS identified and quantified 2799 proteins. Hierarchical clustering revealed distinct protein expression profiles between the PA and control groups (Figure 1A), indicating significant proteomic alterations following PA infection. Differential expression analysis identified 312 significantly altered proteins (FC > 1.5, P < 0.05). The volcano plot shows 59 upregulated and 253 downregulated proteins in the PA group (Figure 1B), suggesting a complex proteomic response to bacterial challenge.

KEGG pathway enrichment analysis revealed that DEPs were most significantly enriched in the "complement and coagulation cascade" and "neutrophil extracellular trap formation" pathways (Figure 1C). Within the NETs formation pathway, both HMGB1 and RAGE were significantly upregulated and showed direct interaction (Figure 1D). Based on these findings, we hypothesized that the HMGB1/RAGE axis plays a crucial role in PA-induced VAP.

HMGB1/RAGE Axis Demonstrates a Significant Negative Correlation with Monocyte Infiltration

Initial differential analysis of immune cell infiltration revealed no significant disparities in the relative proportions of various immune cell populations between the experimental groups (Figure 2A and B). However, correlation analysis revealed a distinct pattern. Lollipop charts show that monocyte abundance was significantly negatively correlated with both AGER and HMGB1 expression (Figures 2C and D, red text indicates $P < 0.05$). Scatter plots confirm this negative correlation, with $R \approx -0.7$ (Figure 2E and F). This suggests that HMGB1/RAGE activation may be associated with monocyte recruitment and consumption in the inflammatory microenvironment.

Bioinformatic Profiling of the Identification of Potential Therapeutic Agents

Drug-target prediction analysis identified potassium nitrate and 2-mercaptoethanol as candidate compounds with high binding affinity to the axis (Figure 3A), suggesting their potential as small-molecule inhibitors. The molecular structure of potassium nitrate is shown in Figure 3B, and the molecular structure of 2-mercaptobenzeneethanol is shown in Figure 3C.

FPS-ZM1 Alleviates Lung Tissue Injury and Systemic Symptoms in Rats

Twenty-four hours after modeling, PA group rats exhibited lethargy, cyanosis, and ocular hemorrhage. Gross morphology showed extensive lung edema and hemorrhage (Figure 4A). HE staining revealed thickened alveolar walls, coalesced alveolar spaces, and inflammatory cell infiltration in the PA group (Figure 4B).

FPS-ZM1 treatment significantly alleviated these pathological changes. Lung wet-to-dry weight ratios (Figure 4C) and histopathological scores (Figure 4D) were significantly lower in the FPS-ZM1+PA group than in the PA group ($P < 0.01$).

FPS-ZM1 Inhibits the Activation of the HMGB1/RAGE Pathway

Immunofluorescence co-localization analysis was performed to validate FPS-ZM1 blockade of the HMGB1/RAGE axis in vivo. HMGB1 fluorescence intensity (Figure 5A) and semi-quantitative analysis (Figure 5B) showed strong signals in the PA group, which were significantly reduced by FPS-ZM1 treatment ($P < 0.01$). Similarly, RAGE fluorescence intensity (Figure 5C) and semi-quantitative analysis (Figure 5D) revealed intense signals in the PA group and marked

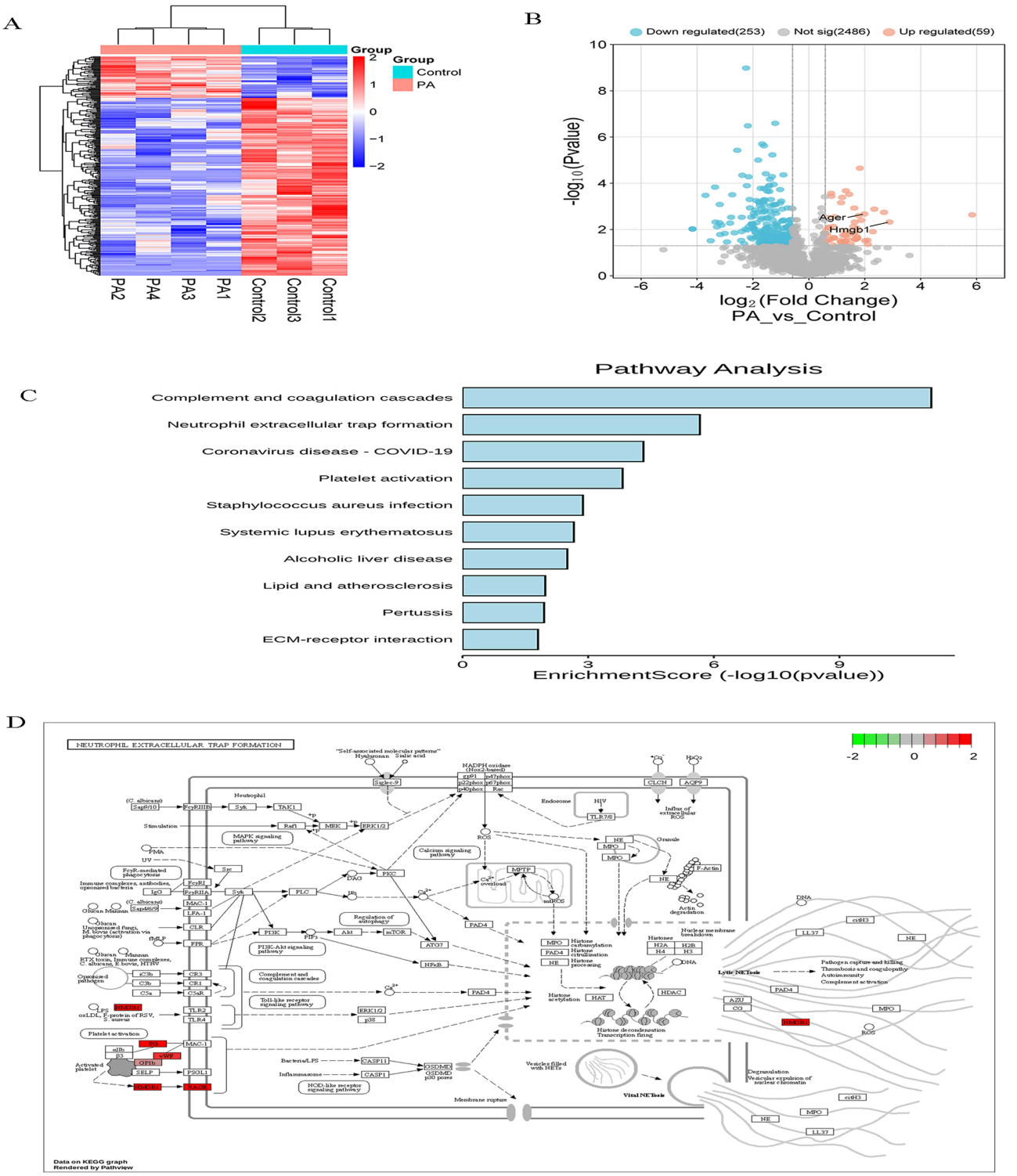

Figure 1 (**A**) Heatmap of DEPs between the PA group and the control group. (**B**) Volcano plot of DEPs between the PA and Control groups with the x-axis representing log2 fold change and the y-axis representing log10(p-value); red dots indicate upregulated DEPs, blue dots indicate downregulated DEPs, and gray dots represent non-differentially expressed proteins. (**C**) KEGG pathway enrichment of DEPs between the PA and Control groups. (**D**) Pathway map of neutrophil extracellular trap (NET) formation.

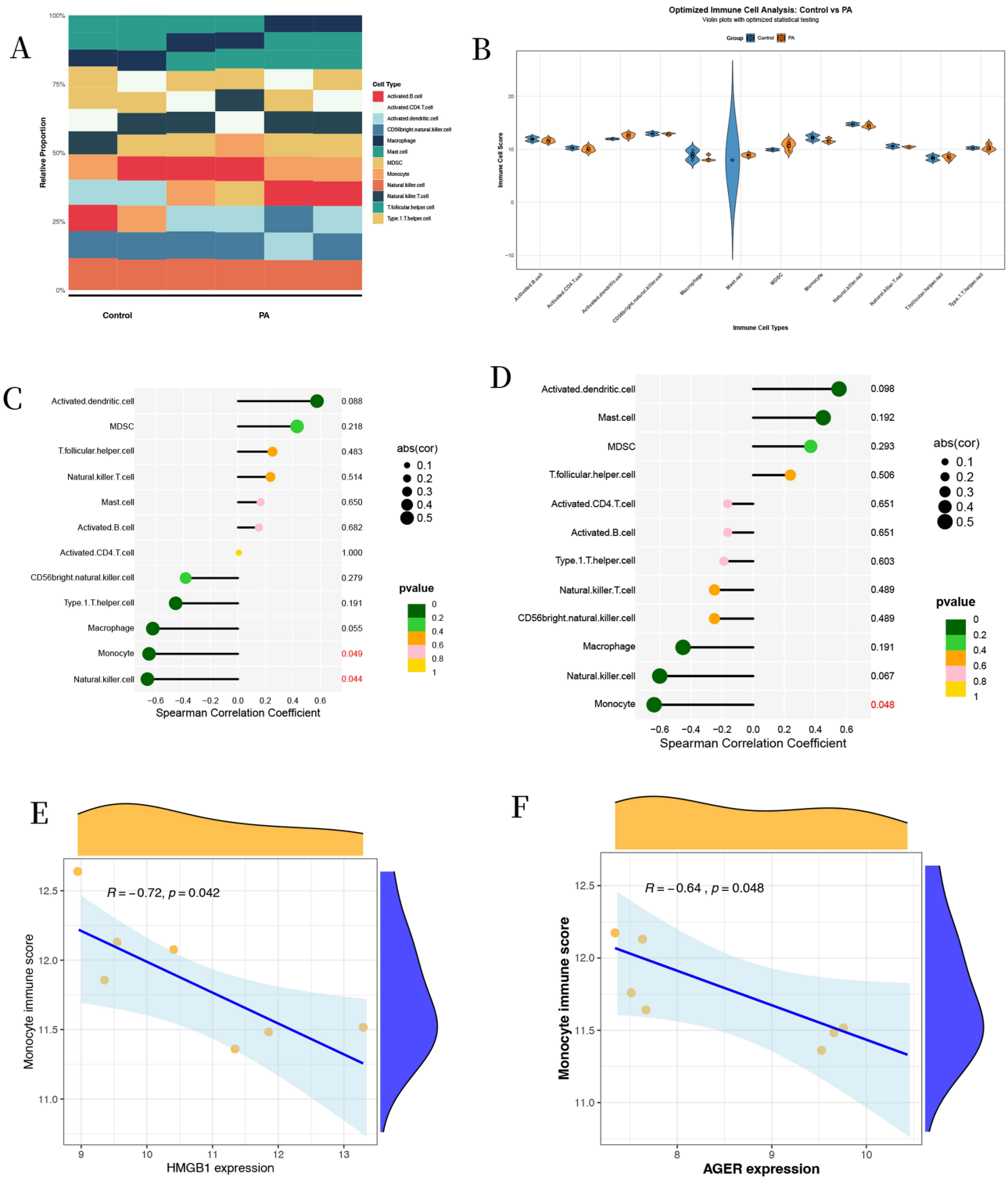

Figure 2 (**A**) Comparison of the relative proportions of immune cell populations between the VAP group and the control group. (**B**) Immune cell infiltration in the VAP and Control groups. (**C** and **D**) Lollipop charts showing the correlation between HMGB1/RAGE expression levels and immune cell abundance. The red text indicates immune cell types with statistically significant correlations ($P < 0.05$) with HMGB1/RAGE expression. (**E** and **F**) Scatter plots depicting the correlation of HMGB1/RAGE expression with monocyte abundance. The correlation coefficient (r) and p-value are indicated.

https://doi.org/10.2147/JIR.S580972

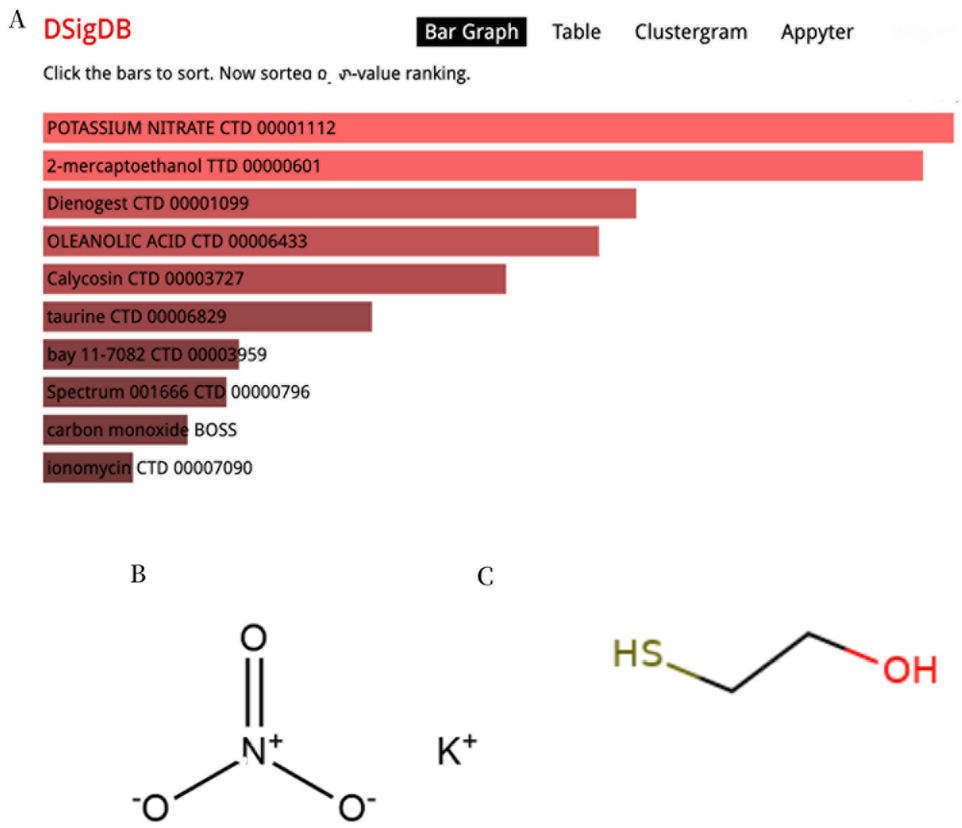

Figure 3 (**A**) Anticipated drugs using DsigDB. (**B**) Molecular structures of the two top-ranked candidate compounds, Potassium nitrate. (**C**) Molecular structures of the two top-ranked candidate compounds, 2-mercaptoethanol.

reduction following FPS-ZM1 treatment ($P < 0.01$). Co-localization of HMGB1 and RAGE was substantially decreased in the treatment group, confirming effective pathway inhibition.

ELISA quantification further confirmed these findings. In serum, HMGB1 (Figure 5E) and RAGE (Figure 5F) levels were significantly elevated in PA-infected rats compared to controls, and were significantly reduced by FPS-ZM1 treatment ($P < 0.01$). In BALF, HMGB1 (Figure 5G) and RAGE (Figure 5H) levels showed the same pattern: PA infection increased both proteins, while FPS-ZM1 treatment attenuated these increases ($P < 0.01$). These results demonstrate that pharmacological blockade of RAGE effectively suppresses HMGB1/RAGE axis activation at both local and systemic levels.

FPS-ZM1 Reduces the Levels of Inflammatory Cytokines in Serum and Lung Tissue

To assess the anti-inflammatory effect of FPS-ZM1, we measured pro-inflammatory cytokines TNF-α, IL-1β, and IL-6 in serum and BALF. In serum, TNF-α (Figure 6A), IL-6 (Figure 6B), and IL-1β (Figure 6C) levels were significantly elevated in the PA group compared to controls. FPS-ZM1 treatment significantly reduced all three cytokines ($P < 0.01$).

In BALF, TNF-α (Figure 6D), IL-6 (Figure 6E), and IL-1β (Figure 6F) levels showed a similar pattern: PA infection induced marked increases, while FPS-ZM1 treatment significantly attenuated these increases ($P < 0.01$). These findings demonstrate that blocking the HMGB1/RAGE axis effectively suppresses both local pulmonary and systemic inflammatory responses in PA-induced VAP.

Discussion

Proteomics, a valuable tool for identifying distinct protein profiles in health and disease, has been successfully applied in numerous studies.[25,26] This study employed an integrated using proteomics and experimental validation to confirm the critical role of the HMGB1/RAGE axis in a PA-induced rat model of VAP. Our findings demonstrate that in this model,

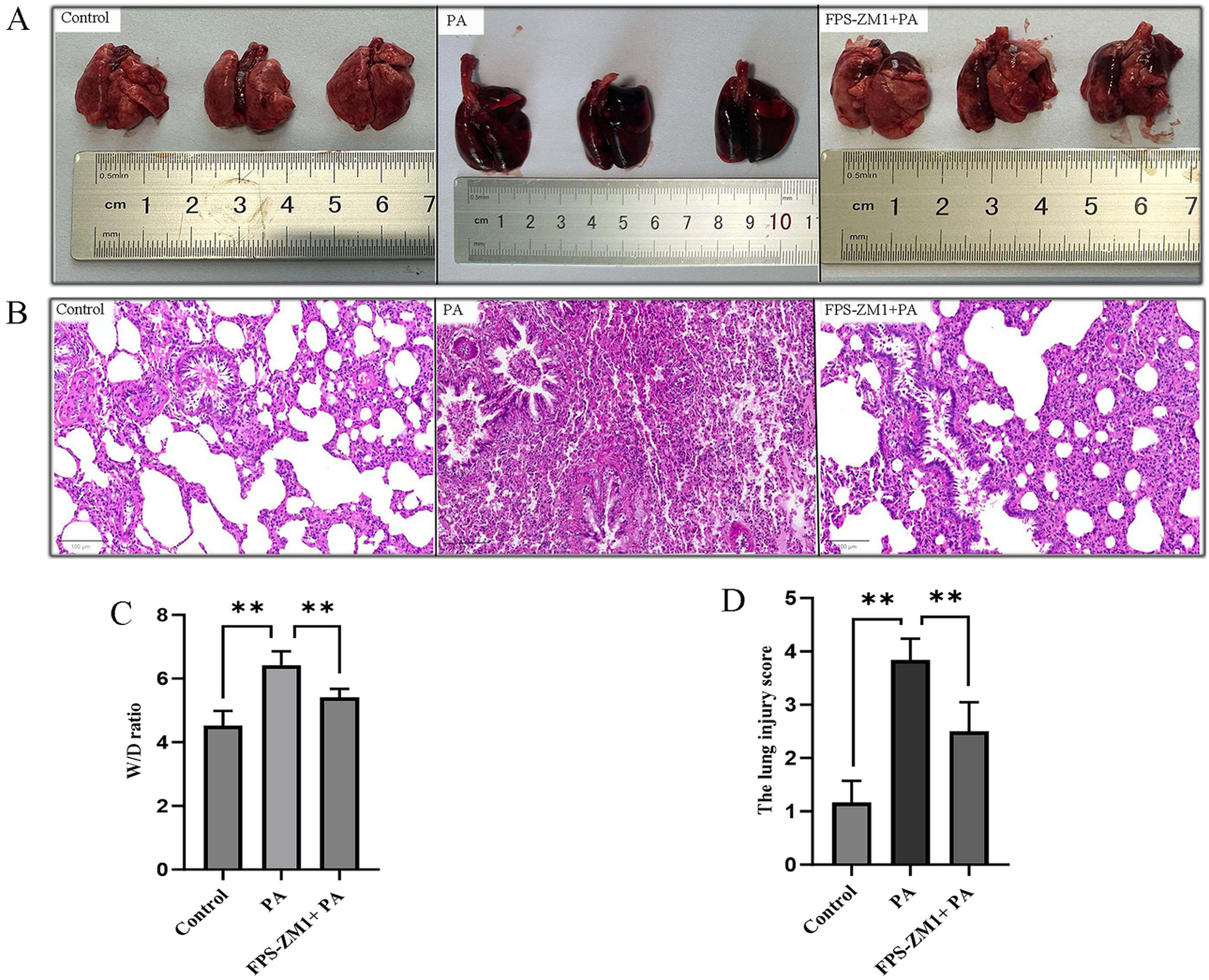

Figure 4 (**A**) Morphology of lung tissue specimens from each group of rats. (**B**) HE staining of lung tissue from each group of rats (10×40 magnification, scale bar = 100 μm). (**C**) Wet-to-dry weight ratios of lung tissue from each group of rats. (**D**) Histopathological scores for lung injury in each group of rats. Data are presented as mean ± SD (n = 6 per group). $^{**}P < 0.01$.

activation of the HMGB1/RAGE axis correlates with both pulmonary and systemic inflammation, and its pharmacological inhibition attenuates lung injury and the release of inflammatory cytokines.

In this study, proteomic analysis identified 312 differentially expressed proteins (DEPs), of which 59 were up-regulated and 253 were down-regulated. Further pathway enrichment analysis revealed that the HMGB1/RAGE axis was enriched in the NETs pathway, with both HMGB1 and its high-affinity receptor RAGE showing not only up-regulated expression but also evidence of direct interaction within this pathway, thereby positioning it as a critical node in the neutrophil-associated inflammatory network. NETs play a complex and dual role in bacterial pneumonia: while they limit bacterial dissemination through synergistic mechanisms including physical entrapment, antimicrobial protein-mediated killing, and nutrient deprivation, their excessive release contributes to substantial lung damage and inflammatory pathology via direct cytotoxicity, pro-thrombotic effects, and by acting as DAMPs that perpetuate inflammation.[27] As a late-phase inflammatory mediator, HMGB1 can be released either passively from infected necrotic cells or actively by activated immune cells.[28,29] Extracellular HMGB1, acting as DAMPs, mediates the onset of a cytokine storm by binding to receptors such as RAGE, TLR2, and TLR4.[30] Following administration of a median lethal dose (LD50) of LPS, serum HMGB1 becomes detectable at 8 hours and increases to a sustained plateau level between 16 and 32 hours post-treatment.[31] In previous sepsis clinical trials, several inhibitors targeting early inflammatory cytokines (eg, TNF-α, IL-1)

https://doi.org/10.2147/JIR.S580972

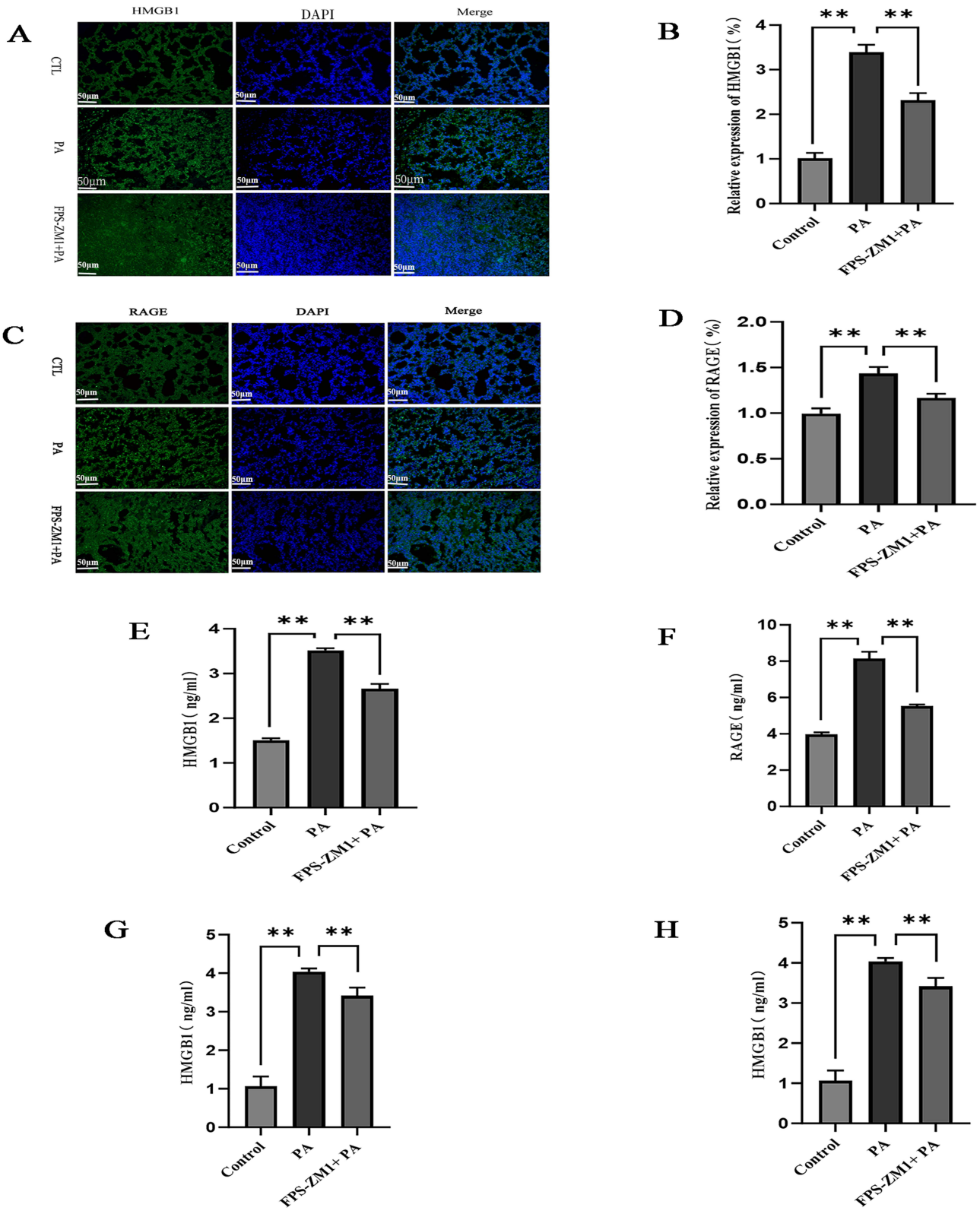

Figure 5 (**A** and **B**) Immunofluorescence intensity and semi-quantitative analysis of HMGB in each group of rats. (**C** and **D**) Immunofluorescence intensity and semi-quantitative analysis of RAGE in each group of rats. (**E** and **F**) Expression levels of HMGB1 and RAGE in the serum of each group of rats. (**G**–**H**) Expression levels of HMGB1 and RAGE in the BALF of each group of rats. $^{**}P < 0.01$.

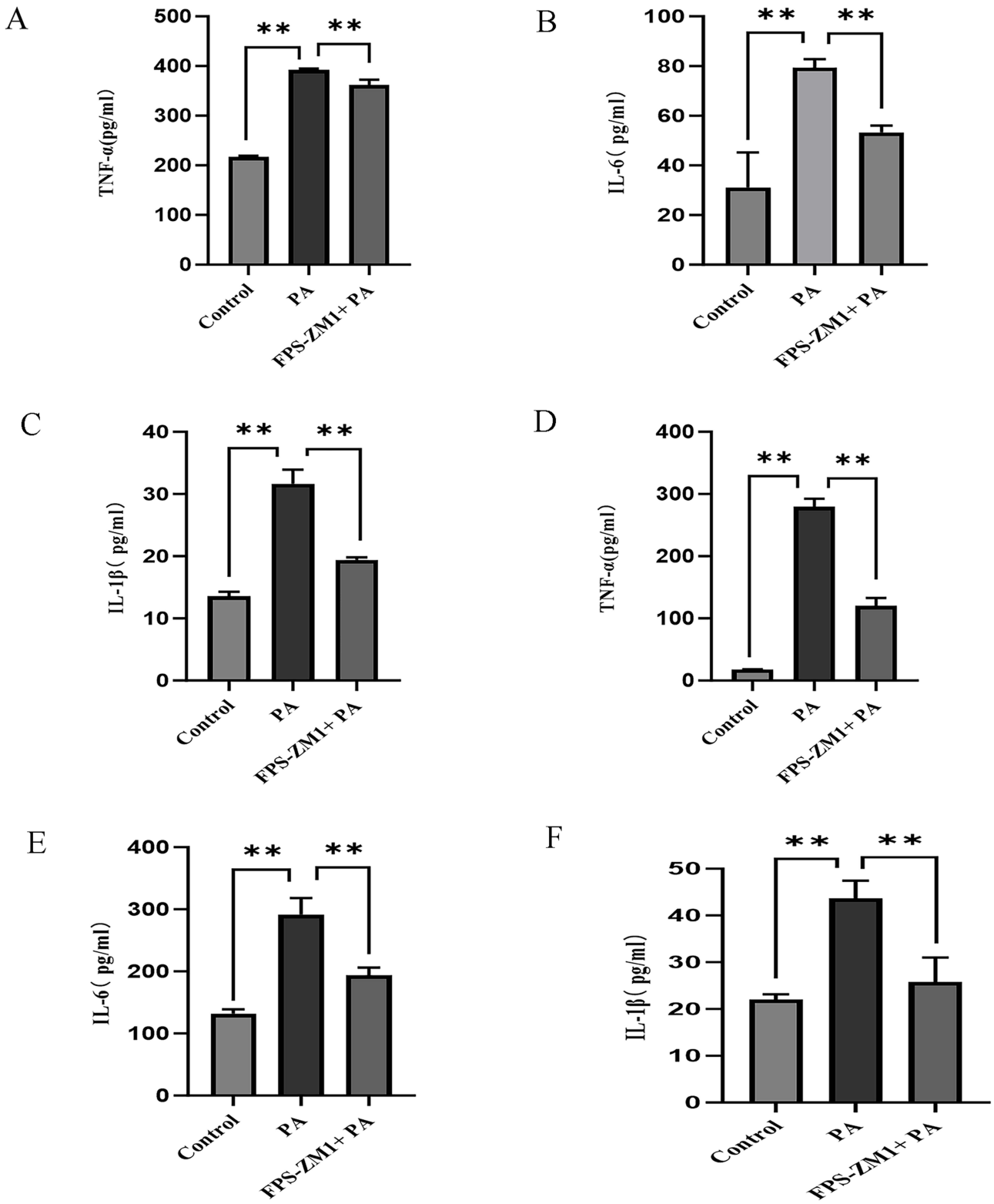

Figure 6 (**A**–**C**) Expression levels of TNF-α, IL-6, and IL-1β in the serum of each group of rats. (**D**–**F**) Expression levels of TNF-α, IL-6, and IL-1β in the BALF of each group of rats. $^{**}P < 0.01$.

https://doi.org/10.2147/JIR.S580972

were tested but failed to achieve desired outcomes, likely due to the rapid kinetics of these cytokines[32,33] Consequently, HMGB1 offers a broader therapeutic window compared to early inflammatory cytokines. Hence, based on the proteomics data, we prioritized this axis over other dysregulated proteins for subsequent experimental validation. The proposed molecular mechanism by which the HMGB1/RAGE axis mediates inflammatory responses in PA-induced VAP is illustrated in Figure 7.

As hypothesized, the expression levels of both HMGB1 and RAGE were significantly elevated in the lung tissue, serum, and BALF of PA-infected rats. Notably, immunofluorescence co-localization confirmed their enhanced expression within lung tissue, and pharmacological blockade with the known RAGE inhibitor FPS-ZM1 effectively reduced this interaction and lowered the levels of both HMGB1 and RAGE in serum and BALF, thereby confirming successful target engagement. Functionally, this inhibition translated into a reduction in lung histopathological injury, a decrease in the wet/dry weight ratio, and an improvement in histopathological scores. Furthermore, treatment with FPS-ZM1 reduced the levels of TNF-α, IL-1β, and IL-6 in both serum and BALF. Collectively, these observations indicate that HMGB1/RAGE signaling contributes to the development of lung injury in this model by amplifying both local and systemic inflammation, whereas blockade of this axis mitigates inflammatory responses at both levels. HMGB1 is known to activate several signaling pathways, including NF-κB, F2/Rho, MAPK, and RhoA/ROCK1, via RAGE, leading to the sustained secretion of inflammatory cytokines.[34–37] Although downstream molecules such as TNF-α, IL-1β, and IL-6 were detectable upon activation of these pathways, the intricate interplay between HMGB1 and RAGE as well as between the HMGB1/RAGE axis and inflammatory cytokines (eg, TNF-α, IL-1β, IL-6) has not been fully clarified in the present study, thus warranting further investigation into their detailed mechanismsOf interest, we observed a significant negative correlation between HMGB1/RAGE expression and monocyte abundance, suggesting a dynamic immunomodulatory role for this axis in the local microenvironment. Specifically, during the early inflammatory phase, HMGB1 acts as an alarmin that recruits monocytes to the site of inflammation upon binding to receptors such as RAGE and activating downstream pathways. However, by 24 hours post-infection, monocyte counts were notably reduced, indicating a process of compensatory rapid consumption. Wang et al[38] found that HMGB1 contributes to LPS-induced lung injury by activating the AIM2 inflammasome in macrophages to induce apoptosis and by promoting the polarization of monocytes/macrophages toward a pro-inflammatory M1 phenotype via the RAGE/NF-κB signaling pathway. Consequently, in this model, activation of the HMGB1/RAGE axis likely drives both the polarization of monocytes/macrophages toward a pro-inflammatory phenotype and their apoptosis, which may explain the observed negative correlation with monocyte abundance and suggests that sustained axis activation could lead to a state of persistent immune dysregulation. Therefore, an additional mechanism of FPS-ZM1 in this model may involve protecting immune cells from exhaustion and death. Collectively, targeting the HMGB1/RAGE axis presents a potential therapeutic strategy to prevent or correct immune dysregulation in this VAP rat model.

Given the significance of the HMGB1/RAGE axis, a network pharmacology-based screening was conducted, identifying potassium nitrate and 2-mercaptoethanol (2-ME) as particularly noteworthy candidate drugs. Nitrate, a biological precursor to nitric oxide (NO), may confer its potential benefits by modulating the HMGB1/RAGE axis. Studies have found that NO from specific sources, such as the endothelial type, negatively regulates both RAGE expression and inflammatory responses. In a rat tMCAo model, blockade with two nitric oxide synthase (NOS) inhibitors revealed that selective inhibition of endothelial NOS (eNOS) exacerbated cerebral infarction, concurrently upregulating

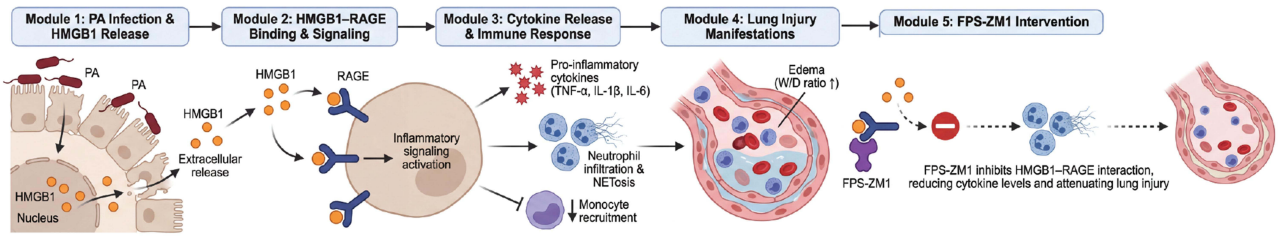

Figure 7 Proposed signaling pathway of HMGB1/RAGE axis in the pathogenesis of Pseudomonas aeruginosa-induced VAP.

mRNA levels of full-length RAGE (fl-RAGE) and pro-inflammatory cytokines (IL-6, TNF-α) in the ischemic cortex and striatum. In contrast, the non-selective NOS inhibitor L-NAME mitigated cortical damage without elevating cortical inflammatory cytokine expression, suggesting that the loss of endogenous protective NO disinhibits the RAGE pathway.[39] Therefore, during the early phase of acute lung injury, exogenous potassium nitrate supplementation may generate a relatively mild and sustained NO flux akin to that from eNOS, which, in contrast to the inflammatory "NO storm" produced by NOS, could exert therapeutic effects in the rat VAP model. Research indicates that the redox state of cysteine residues in extracellular HMGB1 dictates its biological effects. Specifically, the disulfide form of HMGB1 activates the TLR4 complex by binding to MD-2. This binding forces the dimerization of two TLR4 chains, forming a composite structure capable of engaging intracellular signaling adaptors, which ultimately drives a potent inflammatory response;[40] In contrast, the reduced form of HMGB1 loses its ability to activate TLR4 and consequently its pro-inflammatory activity.[41] Within this pathological context, the therapeutic potential of 2-ME as a potent reducing agent is highlighted. Its mechanism of action does not involve antagonizing HMGB1 but rather chemically modifying it. Specifically, 2-ME reduces the excessively accumulated pro-inflammatory disulfide HMGB1 to the chemotactic, fully reduced form. This conversion may shift the local immune response from a TLR4-mediated destructive pattern dominated by inflammation and cell death toward a CXCR4-mediated mode that favors directed cell migration and clearance.[42] Therefore, 2-ME represents a novel class of intervention strategies that function by modulating the immune response via redox modification of HMGB1, offering a new perspective distinct from traditional receptor blockade for the treatment of HMGB1-driven inflammatory diseases.

Nonetheless, this study has several limitations. First, the use of a single PA strain and a standardized rat model may not fully capture the heterogeneity of human VAP. Second, the observation period was limited to 24 hours post-infection, precluding the investigation of longer-term effects. Finally, potassium nitrate and 2-ME are predicted compounds whose specific mechanisms of action, as well as the mechanistic link between the HMGB1/RAGE axis and cytokine production, remain to be elucidated and warrant further investigation.

Conclusion

Our experimental results demonstrate that the HMGB1/RAGE axis is activated and contributes to both lung injury and systemic inflammation in the PA-induced rat VAP model, and that inhibition of this axis alleviates these pathological responses. Infiltration analysis of monocytes further revealed a negative regulatory relationship with the HMGB1/RAGE axis, suggesting its modulatory role in immune cell recruitment within this model. Additionally, immunopharmacological prediction identified potassium nitrate and 2-mercaptoethanol as potential small molecules targeting the HMGB1/RAGE axis. Although these findings do not yet support direct clinical application, they provide a rationale for further investigation into modulating the HMGB1/RAGE axis as part of a multi-target therapeutic strategy for VAP.

Use of Artificial Intelligence Tools

No artificial intelligence tools were used.

Data Sharing Statement

The data that support the findings of this study are available from the corresponding author upon reasonable request. However, the proteomics data cannot be shared at this time, as they are still undergoing in-depth mining and analysis.

Ethical Approval and Informed Consent

All experimental operations were conducted following the "Guide for the Care and Use of Laboratory Animals" and approved by the Experimental Animal Ethics Committee of the Zunyi Medical University (Approval No: [2023] 2023ZH0042). All experimental procedures and operations were strictly carried out in accordance with the ARRIVE guidelines.

Patient Public Statement

There is no applicable content.

Acknowledgments

There is no applicable content.

Author Contributions

Xuanli Huang and Mingpeng Feng contributed equally to this work as co-first authors.

Xuanli Huang: Conceptualization, Formal analysis, Writing - Original Draft, Visualization.

Mingpeng Feng: Software, Data Curation, Writing - Original Draft.

Siqi Li: Investigation, Writing - Review & Editing, Resources. Chengjun Huang: Visualization, Methodology, Writing - Review & Editing.

Yu Xu: Investigation, Data Curation, Writing - Review & Editing.

Haifei Cheng: Formal analysis, Writing - Review & Editing.

Le Mi: Methodology, Software. Writing - Review & Editing.

Hongman Wang: Supervision, Project administration, Funding acquisition, Writing - Review & Editing.

All authors gave final approval of the version to be published; have agreed on the journal to which the article has been submitted; and agree to be accountable for all aspects of the work.

Funding

This research was funded by the National Natural Science Foundation of the People's Republic of China (Project Number: 81960023).

Disclosure

The authors declare no conflicts of interest.

References

1. Papazian L, Klompas M, Luyt CE. Ventilator-associated pneumonia in adults: a narrative review. *Intensive Care Med*. 2020;46(5):888–906. doi:10.1007/s00134-020-05980-0
2. Luyt CE, Hékimian G, Koulenti D, Chastre J. Microbial cause of ICU-acquired pneumonia: hospital-acquired pneumonia versus ventilator-associated pneumonia. *Curr Opin Crit Care*. 2018;24(5):332–338. doi:10.1097/MCC.0000000000000526
3. Leme SP, Lorenzo B, Rocco Patricia RM, et al. Physiological and pathophysiological consequences of mechanical ventilation. *Semin Respir Crit Care Med*. 2022;43(3):321–334. doi:10.1055/s-0042-1744447
4. Sandra-Maria W, Mario M, Geraldine N, et al. Ventilator-induced lung injury is aggravated by antibiotic mediated microbiota depletion in mice. *Crit Care*. 2018;22(1):282. doi:10.1186/s13054-018-2213-8
5. Katira Bhushan H, Giesinger Regan E, Doreen E, et al. Adverse heart-lung interactions in ventilator-induced lung injury. *Am J Respir Crit Care Med*. 2017;196(11):1411–1421. doi:10.1164/rccm.201611-2268OC
6. Tang D, Kang R, Zeh HJ, Lotze MT. The multifunctional protein HMGB1: 50 years of discovery. *Nat Rev Immunol*. 2023;23(12):824–841. doi:10.1038/s41577-023-00894-6
7. Chen R, Kang R, Tang D. The mechanism of HMGB1 secretion and release. *Exp Mol Med*. 2022;54(2):91–102. doi:10.1038/s12276-022-00736-w
8. Wang S, Zhang Y. HMGB1 in inflammation and cancer. *J Hematol Oncol*. 2020;13(1):116. doi:10.1186/s13045-020-00950-x
9. Liu T, Son M, Diamond B. HMGB1 in Systemic Lupus Erythematosus. *Front Immunol*. 2020;11:1057. doi:10.3389/fimmu.2020.01057
10. Pellegrini L, Foglio E, Pontemezzo E, Germani A, Russo MA, Limana F. HMGB1 and repair: focus on the heart. *Pharmacol Ther*. 2019;196:160–182. doi:10.1016/j.pharmthera.2018.12.005
11. Gaikwad S, Puangmalai N, Bittar A, et al. Tau oligomer induced HMGB1 release contributes to cellular senescence and neuropathology linked to Alzheimer's disease and frontotemporal dementia. *Cell Rep*. 2021;36(3):109419. doi:10.1016/j.celrep.2021.109419
12. Du S, Zhang X, Jia Y, et al. Hepatocyte HSPA12A inhibits macrophage chemotaxis and activation to attenuate liver ischemia/reperfusion injury via suppressing glycolysis-mediated HMGB1 lactylation and secretion of hepatocytes. *Theranostics*. 2023;13(11):3856–3871. doi:10.7150/thno.82607
13. Bangert A, Andrassy M, Müller AM, et al. Critical role of RAGE and HMGB1 in inflammatory heart disease. *Proc Natl Acad Sci U S A*. 2016;113(2):E155–64. doi:10.1073/pnas.1522288113
14. Mahadev BS, Nyzil M, Karriker Locke A, et al. Ethyl pyruvate reduces organic dust-induced airway inflammation by targeting HMGB1-RAGE signaling. *Respir Res*. 2019;20(1):27. doi:10.1186/s12931-019-0992-3
15. Rojas A, Lindner C, Schneider I, Gonzalez I, Uribarri J. The RAGE axis: a relevant inflammatory hub in human diseases. *Biomolecules*. 2024;14(4):412. doi:10.3390/biom14040412
16. Oczypok EA, Perkins TN, Oury TD. All the "RAGE" in lung disease: the receptor for advanced glycation endproducts (RAGE) is a major mediator of pulmonary inflammatory responses. *Paediatr Respir Rev*. 2017;23:40–49. doi:10.1016/j.prrv.2017.03.012
17. Hudson BI, Lippman ME. Targeting RAGE signaling in inflammatory disease. *Annu Rev Med*. 2018;69(1):349–364. doi:10.1146/annurev-med-041316-085215

18. Yan YH, Sun XD, Zhang YT, Jin TT, Ying LJ. Role of the HMGB1/TLR4 signaling pathway in ventilator-associated pneumonia in rats. *Chin J Nosocomiol*. 2021;31(6):811–815.
19. Antonelli A, Di Maggio S, Rejman J, et al. The shedding-derived soluble receptor for advanced glycation endproducts sustains inflammation during acute Pseudomonas aeruginosa lung infection. *Biochim Biophys Acta Gen Subj*. 2017;1861(2):354–364. doi:10.1016/j.bbagen.2016.11.040
20. Patel Vivek S, Sitapara Ravikumar A, Ashwini G, et al. High mobility group box-1 mediates hyperoxia-induced impairment of Pseudomonas aeruginosa clearance and inflammatory lung injury in mice. *Am J Respir Cell Mol Biol*. 2013;48(3):280–287. doi:10.1165/rcmb.2012-0279OC
21. Lihong Y, Haijin Z, Haixiong T, et al. The receptor for advanced glycation end products is required for β-catenin stabilization in a chemical-induced asthma model. *Br J Pharmacol*. 2016;173(17):2600–2613. doi:10.1111/bph.13539
22. Arthur L, Chet B, Helga T, et al. The molecular signatures database (MSigDB) hallmark gene set collection. *Cell Syst*. 2015;1(6):417–425. doi:10.1016/j.cels.2015.12.004
23. Nicole R. Expanded CIBERSORTx. *Nat Methods*. 2019;16(7):577. doi:10.1038/s41592-019-0486-8
24. Barbie David A, Pablo T, Boehm Jesse S, et al. Systematic RNA interference reveals that oncogenic KRAS-driven cancers require TBK1. *Nature*. 2009;462(7269):108–112. doi:10.1038/nature08460
25. Min Z, Zhang Y, Yang J, et al. YAP promotes autophagy and progression of gliomas via upregulating HMGB1. *J Exp Clin Cancer Res*. 2021;40(1):99. doi:10.1186/s13046-021-01897-8
26. Piao L, Qian Z, Tian-Yu Z, et al. Celastrol mitigates inflammation in sepsis by inhibiting the PKM2-dependent Warburg effect. *Mil Med Res*. 2022;9(1):22. doi:10.1186/s40779-022-00381-4
27. Zhiwei L, Mingshan X, Mingqing L, et al. Multi-omics driven biomarker discovery and pathological insights into Pseudomonas aeruginosa pneumonia. *BMC Infect Dis*. 2025;25(1):745. doi:10.1186/s12879-025-11119-7
28. Wang H, Bloom O, Zhang M, et al. HMG-1 as a late mediator of endotoxin lethality in mice. *Science*. 1999;285(5425):248–251. doi:10.1126/science.285.5425.248
29. Paola S, Tom M, Bianchi Marco E. Release of chromatin protein HMGB1 by necrotic cells triggers inflammation. *Nature*. 2002;418(6894):191–195. doi:10.1038/nature00858
30. Salminen A. Redox-sensitive high mobility group box 1 (HMGB1) is a multifunctional regulator of cellular senescence, inflammation, and immunosuppression: impact on the aging process. *Ageing Res Rev*. 2026;113:102926. doi:10.1016/j.arr.2025.102926
31. Wang H, Yang H, Czura CJ, et al. HMGB1 as a late mediator of lethal systemic inflammation. *Am J Respir Crit Care Med*. 2001;164(10 Pt 1):1768–1773. doi:10.1164/ajrccm.164.10.2106117
32. Calandra T, Baumgartner JD, Grau GE, et al; Swiss-Dutch J5 immunoglobulin study group. Prognostic values of tumor necrosis factor/cachectin, interleukin-1, interferon-alpha, and interferon-gamma in the serum of patients with septic shock. *J Infect Dis*. 1990;161(5):982–987. doi:10.1093/infdis/161.5.982
33. Marks JD, Marks CB, Luce JM, et al. Plasma tumor necrosis factor in patients with septic shock. Mortality rate, incidence of adult respiratory distress syndrome, and effects of methylprednisolone administration. *Am Rev Respir Dis*. 1990;141(1):94–97. doi:10.1164/ajrccm/141.1.94
34. Jing G, Zhuo Z, Jia-Yi Y, et al. Inflammation and coagulation abnormalities via the activation of the HMGB1-RAGE/NF-κB and F2/Rho pathways in lung injury induced by acute hypoxia. *Int J Mol Med*. 2023;52(2). doi:10.3892/ijmm.2023.5270
35. Jinxu W, Yueyang X, Tiantian C, et al. Dexmedetomidine attenuates perioperative neurocognitive disorders by suppressing hippocampal neuroinflammation and HMGB1/RAGE/NF-κB signaling pathway. *Biomed Pharmacother*. 2022;150:113006. doi:10.1016/j.biopha.2022.113006
36. Kexin X, Song X, Jin W, et al. Investigation of glaucocalyxin A mechanism in alleviating atopic dermatitis via the HMGB1-RAGE-RhoA/ROCK1-mediated mitochondrial pathway. *FASEB J*. 2025;39(24):e71377. doi:10.1096/fj.202503063R
37. Justyna A, Sylwia R, Magdalena W, et al. HMGB1-dependent signaling in the regulation of mast cell activity during inflammation. *Front Immunol*. 2025;16:1643427. doi:10.3389/fimmu.2025.1643427
38. Jing W, Ruiting L, Zhiyong P, et al. HMGB1 participates in LPS-induced acute lung injury by activating the AIM2 inflammasome in macrophages and inducing polarization of M1 macrophages via TLR2, TLR4, and RAGE/NF-κB signaling pathways. *Int J Mol Med*. 2020;45(1):61–80. doi:10.3892/ijmm.2019.4402
39. Rosaria G, Chiara D, Maria ZA, et al. Modulation of cerebral RAGE expression following nitric oxide synthase inhibition in rats subjected to focal cerebral ischemia. *Eur J Pharmacol*. 2017;800:16–22. doi:10.1016/j.ejphar.2017.02.008
40. Huan Y, Haichao W, Zhongliang J, et al. MD-2 is required for disulfide HMGB1-dependent TLR4 signaling. *J Exp Med*. 2015;212(1):5–14. doi:10.1084/jem.20141318
41. Huan Y, Peter L, Lars O, et al. Redox modifications of cysteine residues regulate the cytokine activity of HMGB1. *Mol Med*. 2021;27(1):58. doi:10.1186/s10020-021-00307-1
42. Seung-Woo K, Hahnbie L, Hye-Kyung L, et al. Neutrophil extracellular trap induced by HMGB1 exacerbates damages in the ischemic brain. *Acta Neuropathol Commun*. 2019;7(1):94. doi:10.1186/s40478-019-0747-x